Suppression of Nonlinear Rotary Slosh Dynamics using the SLS Adaptive Augmenting Control System Demonstration on a Quadcopter Testbed

Jing Pei*
NASA Langley Research Center, Hampton, Virginia, 23681

Andrew Puetz†
South Dakota State University, Brookings, South Dakota, 57007

Camilo Duarte‡
Georgia Institute of Technology, Atlanta, Georgia, 30332

Luke Miller§, Paul Rothhaar¶
NASA Langley Research Center, Hampton, Virginia, 23681

Liquid propellant makes up a significant portion of the total weight for large launch vehicles such as Saturn V, Space Shuttle, and the Space Launch System. Careful attention must be given to the influence of fuel slosh motion on the stability of the vehicle in the design of the Flight Control System (FCS). Historically, there have been instances where a poorly designed FCS in addition to a lack of passive damping have caused the slosh mass to drive the launch vehicle unstable. The dynamics behind controlling a quadcopter/hanging mass configuration is analogous to that of controlling the attitude of a rocket with a single propellant tank. This offers an excellent platform to assess the effectiveness of the SLS Adaptive Augmenting Controller in suppressing slosh instability in real-time. The flight test experiments were carried out at the NASA Langley Research Center's Autonomy Incubator. Both simulation and flight data are presented in this paper.

I. Introduction

Liquid propellant makes up a significant portion, as much as 90%,[1] of the launch vehicle gross weight during liftoff. The effect of fuel sloshing on vehicle dynamics and control must be taken into consideration in the design of the flight control system. This is especially true for propellant tanks with large diameters in which the frequencies of the slosh masses approach the rigid body control frequency. A poorly designed flight control system can cause continuous excitation of the slosh dynamics, making the closed-loop system unstable. In 2007, the SpaceX Falcon demonstration flight II[2] exhibited a noticeable slow divergent oscillation in the roll channel of the upper stage control system. The instability grew and manifested itself in pitch and yaw until second stage engine shutdown. The instability ultimately prevented the vehicle from reaching its intended orbit.

Typically in the formulation of the linearized equations of motion for a launch vehicle,[3,4] the slosh dynamics are treated as either a spring-mass damper or rigid pendulum. In both formulations, the motion is considered to be planar and the displacement of the slosh element is assumed to be small. To more accurately represent slosh dynamics in cylindrical tanks a spherical pendulum model can used.[5–8] A spherical pendulum

*Aerospace Engineer, Systems Analysis and Concepts Directorate, Vehicle Analysis Branch
†Spring Research Intern, Systems Analysis and Concepts Directorate, Vehicle Analysis Branch
‡Spring Research Intern, Systems Analysis and Concepts Directorate, Vehicle Analysis Branch
§Aerospace Engineer, Flight Dynamics Branch
¶Aerospace Engineer, Dynamics and Control Branch

is known to have several instabilities[7] observed in liquid inside an axisymmetric tank including: nonlinear coupling between the wave motion parallel or perpendicular to the plane of excitation, and swirling motions. In this study, a quadcopter plus hanging mass configuration was used to mimic the rotary slosh behaviors of a launch vehicle with liquid propellant inside a cylindrical tank. The two systems are dynamically similar in that the objective of the controller is to stabilize the vehicle and respond to guidance commands while suppressing the effects of slosh dynamics. In addition, both systems allocate commands to the control effectors located at the base of the vehicle. Figure 1 is an illustration showing the similarities between the two systems. This study builds on previous work[9] where a double pendulum/pole-cart configuration was used to demonstrate propellant slosh instability on an aerodynamic unstable rocket.

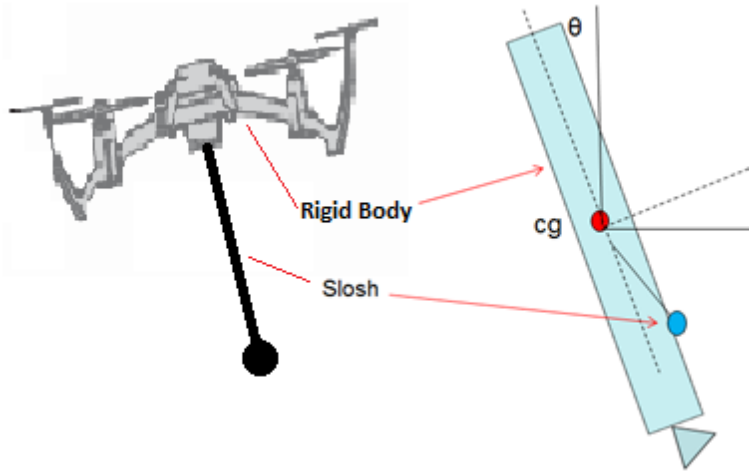

Figure 1. Dynamic Similarities

The second major objective is to demonstrate the ability of NASA's Space Launch System (SLS) Adaptive Augmenting Control (AAC) algorithm[10–15] in suppressing propellant slosh instability by intentionally driving the slosh mass unstable. SLS program baseline flight dynamic simulation models do not take into consideration the nonlinear cross-axis coupling effects in the slosh dynamics. As a result, there are minimal studies that analyzes the response of the AAC to the nonlinear cross-axis coupling effects, especially when the slosh mass becomes unstable. Current study aims to address this issue and is also a follow-on to two previous works[16,17] where the AAC algorithm was applied to an inverted pendulum-cart platform and the attitude dynamics of a quadcopter. This paper is organized as follows: Section II derives the set of full nonlinear equations of motion for the quadcopter/hanging mass system. Section III describes the design of the baseline two-loop linear controller for the quadcopter/hanging mass testbed. Nominal stability margins are provided along with Nichols Charts illustrating the dynamic similarities between the quadcopter/hanging mass testbed and a launch vehicle with a single propellant tank. The AAC algorithm modified for the quadcopter/hanging mass parameters is presented. Section IV discusses the experimental setup. Section V shows both simulation and experiment results in which the slosh mass was intentionally driven unstable and the AAC was activated to suppress the instability. Conclusions are presented in Sec. VI.

II. Quad hanging mass dynamics

Lagrange's method[8,18] was used to derive the equations of motion for the quadcopter/hanging mass system. The hanging mass is treated as a point mass attached at the end of a massless rod. The derivation closely resembles that of a classical spherical pendulum.[5,8] The generalized coordinates are x_q, y_q, and z_q representing the position states of the quadcopter and two spherical angles, θ and ϕ, to describe the states of the hanging mass. Figure 2 is a schematic showing the generalized coordinates. The objective of this study is to analyze the potential unstable interaction between the quadcopter translational dynamics with the dynamics of the hanging mass. The attitude states are not included in the derivation here because they serve as inputs to the translation dynamics.

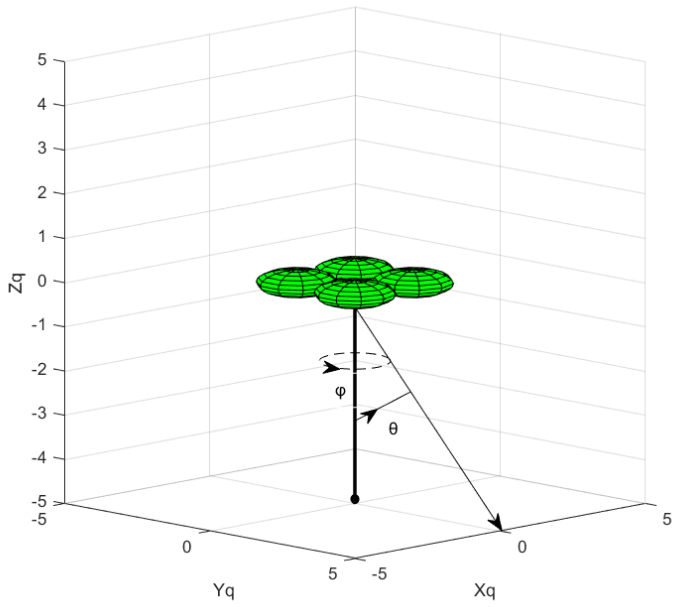

Figure 2. Generalized Coordinates

The position of the hanging mass is given by the following equations:

$$\begin{aligned} x_p &= x_q + L\sin\theta\cos\phi \\ y_p &= y_q + L\sin\theta\sin\phi \\ z_p &= z_q - L\cos\theta \end{aligned} \tag{1}$$

where L is the length of the pendulum. The kinetic energy (T) and potential energy (V) of the system consists of the quadcopter and the pendulum. m_q is the mass of the quadcopter and m_p is the mass of the hanging mass.

$$\begin{aligned} T = \frac{1}{2}m_q(\dot{x_q}^2 + \dot{y_q}^2 + \dot{z_q}^2) + \frac{1}{2}m_p(\dot{x_q} - L\dot{\phi}\sin\theta\sin\phi + L\dot{\theta}\cos\theta\cos\phi)^2 \\ + \frac{1}{2}m_p(\dot{y_q} + L\dot{\phi}\sin\theta\cos\phi + L\dot{\theta}\cos\theta\sin\phi)^2 + \frac{1}{2}m_p(\dot{z_q} + L\dot{\theta}\sin\theta)^2 \end{aligned} \tag{2}$$

$$V = m_q g z_q + m_p g(z_q - L\cos\theta) \tag{3}$$

To derive the full nonlinear equations of motion, substitute T and V into Eq. 4

$$\begin{aligned} \mathscr{L} &= T - V \\ \frac{d}{dt}\left(\frac{\partial \mathscr{L}}{\partial \dot{q}}\right) - \frac{\partial \Gamma}{\partial q} &= Q \end{aligned} \tag{4}$$

here $\mathscr{L}$ is the Lagrangian, q represents the generalized coordinates: $[x_q\ y_q\ z_q\ \theta\ \phi]^T$, and Q represents the generalized forces. The set of nonlinear differential equations are shown below in a matrix format:

$$\begin{bmatrix} (m_q+m_p) & 0 & 0 & Lm_p\cos\theta\cos\phi & -Lm_p\sin\theta\sin\phi \\ 0 & (m_q+m_p) & 0 & Lm_p\cos\theta\sin\phi & Lm_p\sin\theta\cos\phi \\ 0 & 0 & (m_q+m_p) & Lm_p\sin\theta & 0 \\ Lm_p\cos\theta\cos\phi & Lm_p\cos\theta\sin\phi & Lm_p\sin\theta & L^2m_p & 0 \\ -Lm_p\sin\theta\sin\phi & Lm_p\sin\theta\cos\phi & 0 & 0 & L^2m_p\sin^2\theta \end{bmatrix} \begin{bmatrix} \ddot{x_q} \\ \ddot{y_q} \\ \ddot{z_q} \\ \ddot{\theta} \\ \ddot{\phi} \end{bmatrix} \tag{5}$$

$$= \begin{bmatrix} U_x + Lm_p(\sin\theta\cos\phi\dot{\phi}^2 + \sin\theta\cos\phi\dot{\theta}^2 + 2\cos\theta\sin\phi\dot{\theta}\dot{\phi}) \\ U_y + Lm_p(\sin\theta\sin\phi\dot{\phi}^2 + \sin\theta\sin\phi\dot{\theta}^2 - 2\cos\theta\cos\phi\dot{\theta}\dot{\phi}) \\ U_z - Lm_p\cos\theta\dot{\theta}^2 - (m_q + m_p)g \\ m_pL(L\dot{\phi}^2\sin\theta\cos\theta - g\sin\theta) - k_1\dot{\theta} \\ -2m_pL^2\sin\theta\cos\theta\dot{\theta}\dot{\phi} - k_2\sin^2\theta\dot{\phi} \end{bmatrix}$$

U_x, U_y, and U_z are the external inputs into the system. k_1 and k_2 are damping coefficients in the θ and ϕ directions respectively. The damping term $-k_2\sin^2\theta\dot{\phi}$ is there to avoid singularity in the solution.[19] For a Single-Input-Single-Output (SISO) linear control design, the y, z, ϕ dynamics are ignored in Eq. 5 subsequently linearized about: $x = 0$, $\theta = 0$, $\dot{x} = 0$, $\dot{\theta} = 0$. This results in a 4th order plant with two poles at the origin of the s-plane and a pair of imaginary poles as shown in Eq. 6. This is analogous to a classic example of an aerodynamically neutral stable rocket with a single propellant tank.[3]

$$\frac{X(s)}{U_x(s)} = \frac{L^2m_ps^2 + k_1s + m_pLg}{s^2\left[(m_T - m_p)m_pL^2s^2 + m_Tk_1s + m_Tm_PLg\right]} \tag{6}$$

where $m_T = m_q + m_p$.

III. Control Design

Dynamics and control of a quadcopter is well known.[17,20] Since the quadcopter can only produce force in the +Z direction of the body frame, for lateral translation (in X and Y) the quadcopter must calculate a desired pitch and roll attitude such that its thrust vector points in the direction of desired travel. Overall the quadcopter receives four commands it allocates to the rotors: thrust, roll, pitch, and yaw torques. For positive thrust, it increases commands to all four motors simultaneously. For positive roll, it increases commands to motor 1 and 4 while decreases commands motor 2 and 3. For positive pitch, it increases commands to motor 3 and 4 while decreases commands motor 1 and 2. For positive yaw, it increases commands to motor 1 and 3 while decreases commands motor 2 and 4. Figure 3 shows the conventions adopted in this work.

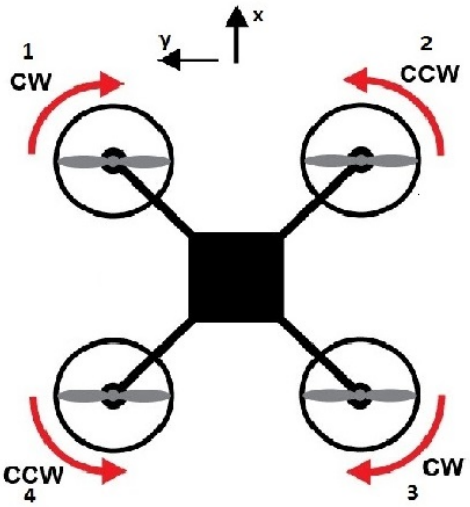

Figure 3. Quadcopter nomenclature

The baseline linear controller consists of a SISO two-loop architecture designed to regulate the lateral translational dynamics (pitch and roll channels) of the quadcopter as shown in Fig. 4. The outer (translational) loop receives position and velocity commands from the guidance system and outputs an attitude command such that the thrust vector points in the desired direction. The inner (attitude) loop receives the attitude command from the outer loop and calculates a torque command to the motors. The objective of current study is to intentionally drive the slosh mass unstable by adjusting the "gain shift" parameter in the translational loop and have the AAC present to suppress that instability. Altitude and yaw channels are

ignored, and therefore not shown in Fig. 4, as the main focus is the adverse coupling between rigid body and slosh dynamics in the pitch and roll channels.

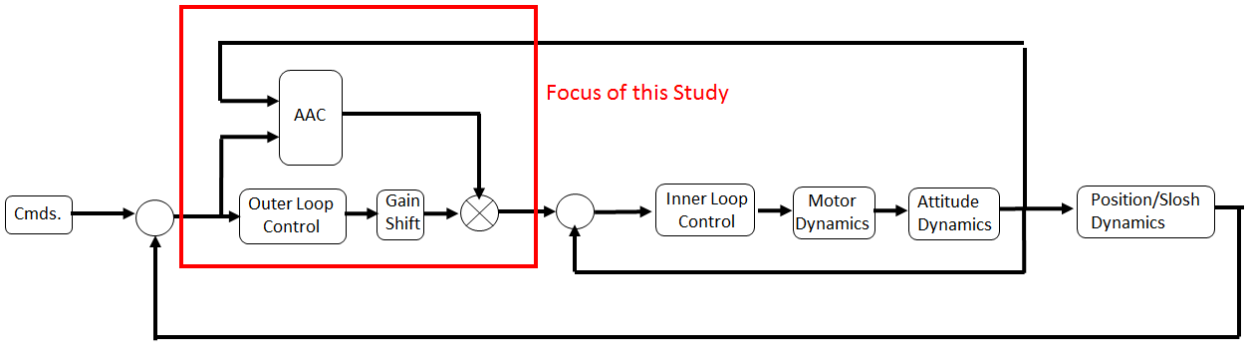

Figure 4. Control Architecture: Pitch and Roll Channels

A. Baseline controller and stability margins

The inner loop was designed first in the two-loop design process and consists of a well-tuned Proportional-Derivative (PD) controller. The quadcopter attitude is available for feedback through a Vicon system.[21] The attitude rates are available for feedback through an on-board IMU. Figure 5 shows the Nichols chart of the inner loop. The attitude loop exemplifies a typical conditionally stable system for which it is stable for only a range of forward loop gain, K_T. A decrease in K_T would cause the system to violate its low frequency gain margin and subsequently cause the quadcopter to tumble. An increase in K_T would cause the system to violate its high frequency gain margin (dictated by the motor dynamics) and manifest itself into a stable limit cycle oscillation in the vehicle roll/pitch attitudes. Reference 17 demonstrated the functionalities of the AAC on the attitude loop of the quadcopter.

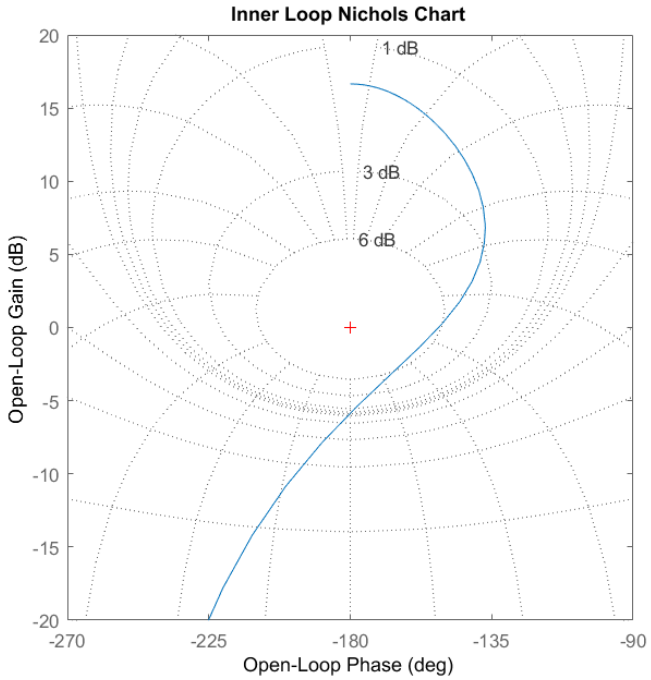

Figure 5. Nichols Chart of the Inner Loop

The outer loop design starts with the inner loop closed and consists of a separate PD controller. Position feedback is available through the Vicon system while velocity feedback comes from state estimates. Figure 6 shows the outer loop Nichols charts with the loop occurring at approximately 0.5 Hz representing the hanging mass/slosh dynamics. This was by design because low frequency slosh modes on launch vehicles generally resides somewhere between 0.3 to 0.5 Hz.[15,22] In this experimental setup, the slosh mass is phase stable[3,9] with respect to control of the quad's translational dynamics, hence the band of frequency response associated with the slosh mode naturally projects away from the (-1,0) critical point. The characteristics of the translational loop Nichols chart is remarkably similar to a low order dynamics model for a launch vehicle[4,23] consisting of rigid body dynamics, second-order actuator model, and a single slosh mode. Table 1 shows the outer loop stability margins along with their crossover frequencies. The high frequency stability margin occurring at 0.525 Hz is driven by the slosh dynamics. The gain crossover frequency occurs at 0.2 Hz which is also remarkably similar to that of SLS and other booster vehicles.[15,22] There does not exist a low frequency gain margin for the outer loop because the attitude loop is closed-loop stable. A substantial decrease in the outer loop K_T would result in large position tracking errors; however, the system would still remain stable in attitude.

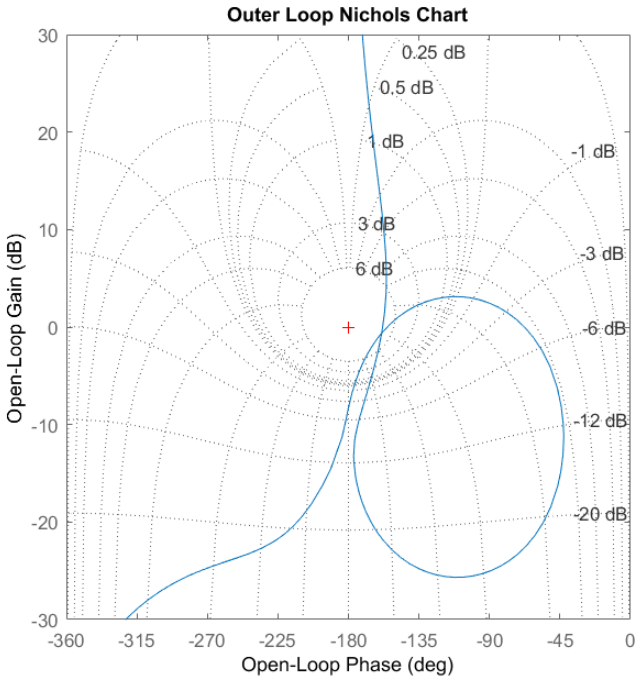

Figure 6. Nichols Chart of the Outer Loop

Table 1. Outer Loop Stability Margins

Margins	Values	Frequency (Hz)
Low Frequency Gain Margin	∞	0
Phase Margin	22 deg	0.2
High Frequency Gain Margin	2.6	0.525

B. Adaptive Augmenting Control

Readers should refer to Refs. 10,12,13,15 for in-depth mathematics, analysis, and discussions behind the AAC algorithm. The AAC algorithm and parameter selection methodology utilized on this platform and experiment was based upon the design and techniques illustrated in SLS program documentation Ref. 15.

Figure 7 is a block diagram representation of the AAC algorithm used in this study. The adaptive law is a balance between low frequency tracking errors (reference model component) with the amount of high frequency contents in the control signal due to undesirable parasitic dynamics (spectral damper component). The three key features of the AAC algorithm are: 1) minimal adaptation when the baseline classical controller is performing nominally ($K_T \approx 1$). 2) Increase system gain in response to excessive command tracking errors in the presence of mismodeled dynamics or in-flight anomalies ($K_T > 1$). 3) Decrease system gain to prevent undesirable high frequency parasitic dynamics (i.e. slosh, flex) from driving the system to instability ($K_T < 1$).

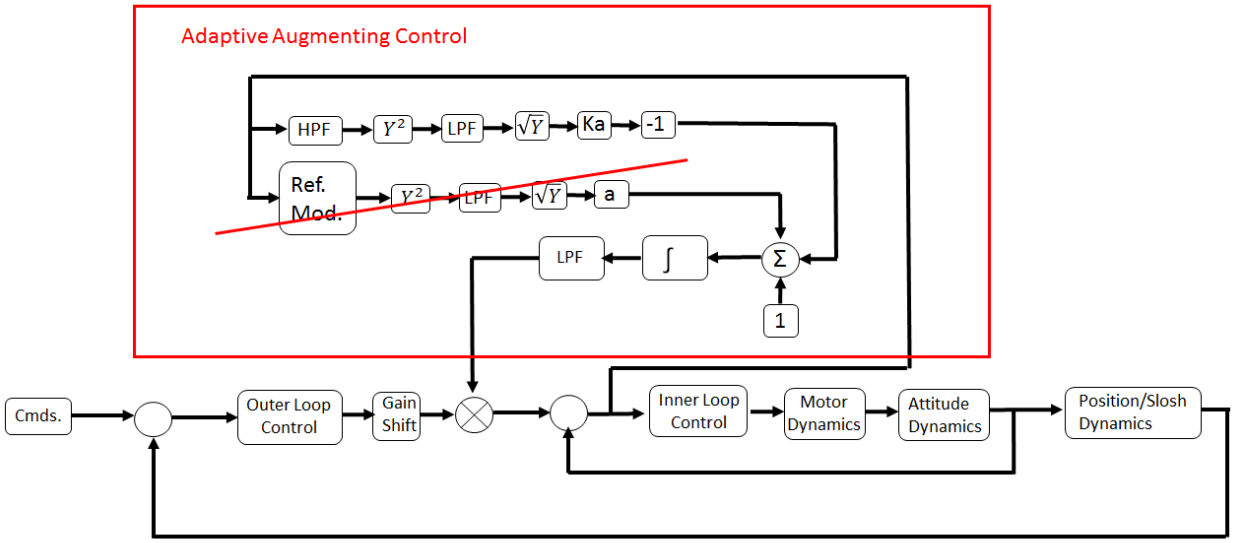

Figure 7. Block Diagram of AAC Architecture

The cutoff frequency that separates the up-band and the down-band portions of the AAC algorithm is known as the "selectivity zero".[15] This design parameter is a function of the various filters and gains shown in Fig. 7. The "selectivity zero", by design, generally occurs close to the gain crossover frequency of the baseline system. For the quadcopter/hanging mass system, the gain crossover frequency of the translational loop occurs around 0.2 Hz as discussed in the previous subsection. Due to the lack of a low frequency instability in the translation loop, only the down-band capability of the AAC algorithm was featured in this study. During the experiments, the "gain shift" parameter was increased in real time that caused the 0.5 Hz slosh mode to become unstable. The AAC is expected to suppress that instability by decreasing the forward loop gain, K_T. Note: because of the remarkable similarities between the translational dynamics of the quadcopter/hanging mass system with the attitude dynamics of SLS with a single slosh tank (both in terms of the characteristics of the frequency response and specific crossover frequencies), the SLS AAC parameters were directly applied to the quadcopter/hanging mass system in this study.

IV. Experimental Setup

Figures 8, 9, 10, and 11 show the quad-rotor setup and the indoor flying area at the NASA Langley Research Center Autonomy Incubator. The setup consists of a host desktop computer and a quad-rotor with an Intel Edison on-board. Not pictured is a Vicon system[21] used to measure the position and attitude of the quad-rotor in a north, east, down frame. The system consisted of 15 cameras placed around the entire flight area at various heights and angles for proper coverage. The software setup consists of DDS[24] Simulink blocks that enable applications to seamlessly share information and work together over a Wi-Fi network. The controller is implemented in Simulink and runs in real time on the host computer. It sends commands to the Intel Edison[25] on-board the quad-rotor and receives IMU and Vicon data regarding the attitude and positional states over Wi-Fi. In order to collect position and altitude data, four silver Vicon spheres are strategically positioned on the quadcopter in an asymmetric configuration. This placement is critical to

obtaining accurate attitude and position data.

Figure 8. Quad-Rotor

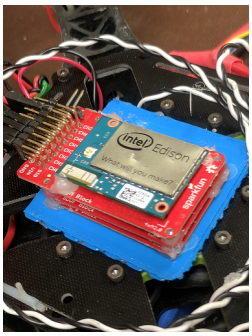

Figure 9. On-board Intel Edison and IMU

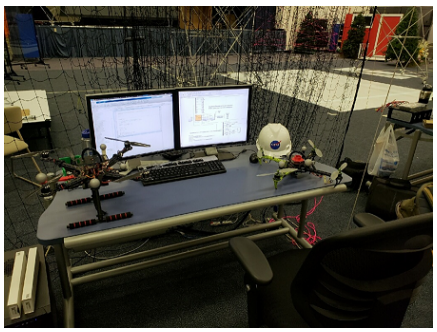

Figure 10. Control Station in AI

Table 2. System Parameters

Quad-Rotor Parameters	Values
Mass	1.5207 kg
I_{xx}	0.0211 kgm^2
I_{yy}	0.0216 kgm^2
I_{zz}	0.01455 kgm^2
Arm Length	0.241 m
Thrust Coefficient	5.8597 x 10e-6 kgm^2
Torque Coefficient	2.9250 x 10e-9 kgm^2
Slosh Mass Length	1 m
Slosh Mass	0.05 kg

Constant parameters include mass, rotational inertia, arm length, thrust and torque coefficients of each rotor and mass/length of the hanging mass. These parameters are tabulated in Table 2.

Figure 11. AI Flight Space

V. Results

A. Simulation Results

The quadcopter was commanded to hover about the origin and the initial conditions for the slosh mass (in radians) were: $\theta = 0.2$ rad, $\dot{\theta} = 0$ rad/s, $\phi = 0$ rad, $\dot{\phi} = 0.6$ rad/s. Figure 12 shows results for the baseline case with AAC off and the "gain shift" parameter set to 1. The set of plots consists of: 1) The quadcopter position in the X-Y plane, 2) The projection of the slosh mass position onto the X-Y plane, 3) Amplitude of the slosh mass, θ, 4) AAC gains. The baseline controller did a good job of keeping the quadcopter hovering about the origin. The passive damping in the system caused the slosh amplitude to decay over time. This is analogous to having baffles on a launch vehicle to passively damp out slosh motion while the controller is attempting to track a desired attitude command.

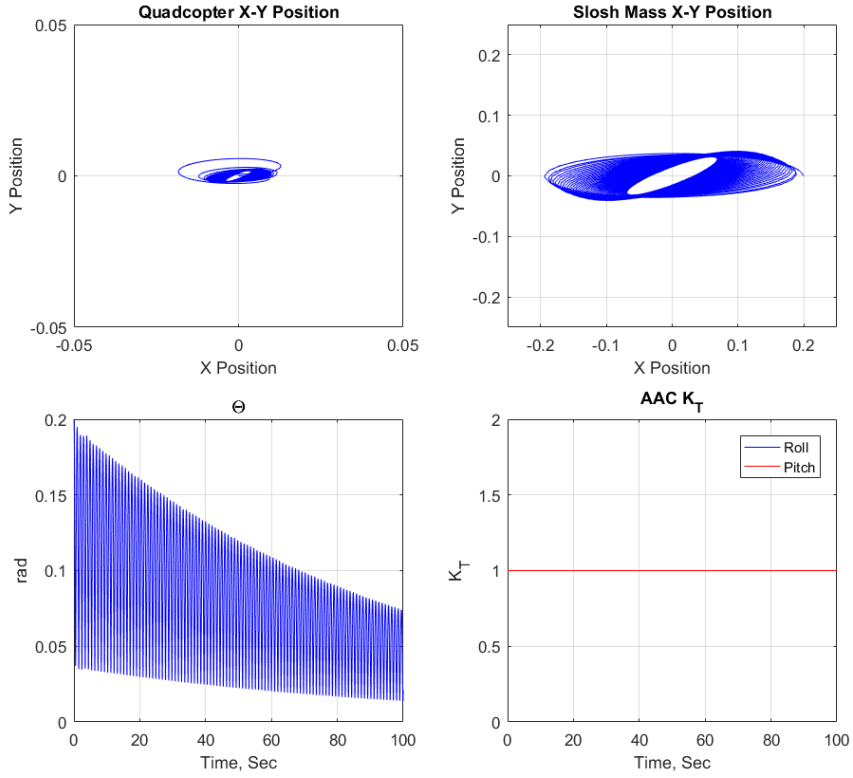

Figure 12. gain shift parameter = 1, AAC OFF

Figure 13 shows results for the AAC off case where the slosh mode was intentionally destabilized by increasing the "gain shift" parameter the high frequency gain margin was violated. The slosh mass amplitude grew from 0.2 rad to 0.25 rad. Due to the nonlinearities in the system and the selected initial conditions, the slosh mass started out with oscillations predominately in X but transitioned gradually to Y. This phenomenon is similar to the nonlinear dynamic behaviors of liquids in cylindrical tanks described in Ref. 1. The inertial coupling between the slosh mass and quadcopter dynamics caused the quadcopter to follow a similar type of instability. This is similar to the slosh instability experienced by the Falcon rocket flight demonstration in 2007.[2]

Figure 14 illustrates the effectiveness of the AAC in suppressing the unstable slosh mode shown in Fig. 13. Here the "gain shift" parameter was again adjusted such that the high frequency gain margin was violated but AAC was activated. AAC sensed large parasitic dynamics errors in the spectral damper channel and immediately reduced K_T in both the pitch and roll channels. The initial reduction in K_T is more aggressive in the pitch channel compare to roll due to the large initial oscillation of the slosh mass in X. As the slosh mass amplitude subsided, the AAC gains crept back towards unity by design.

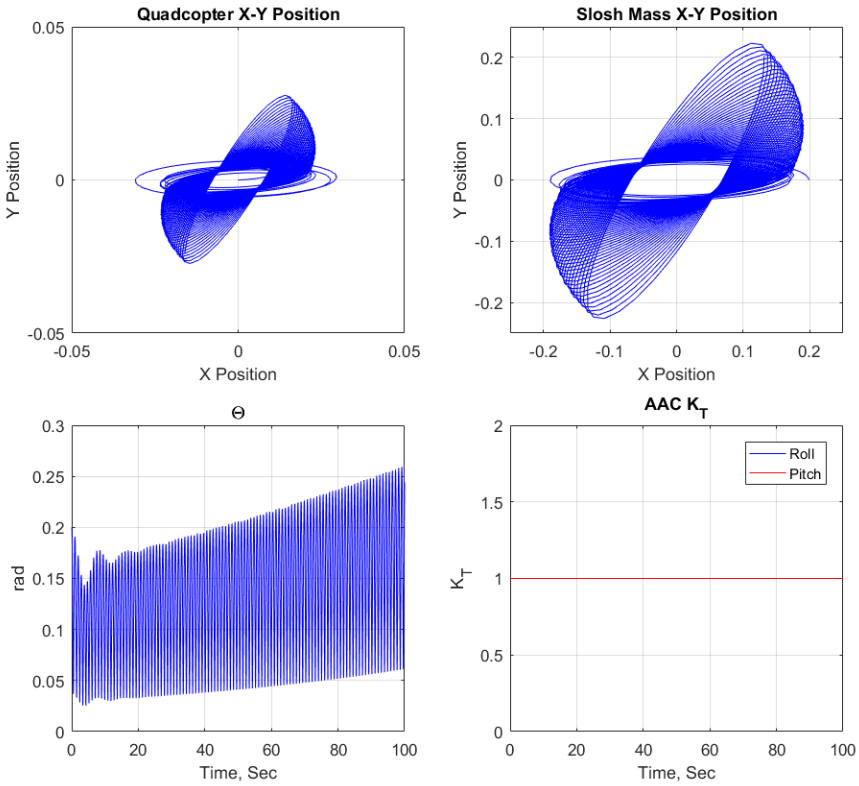

Figure 13. gain shift parameter = 2.3, AAC OFF

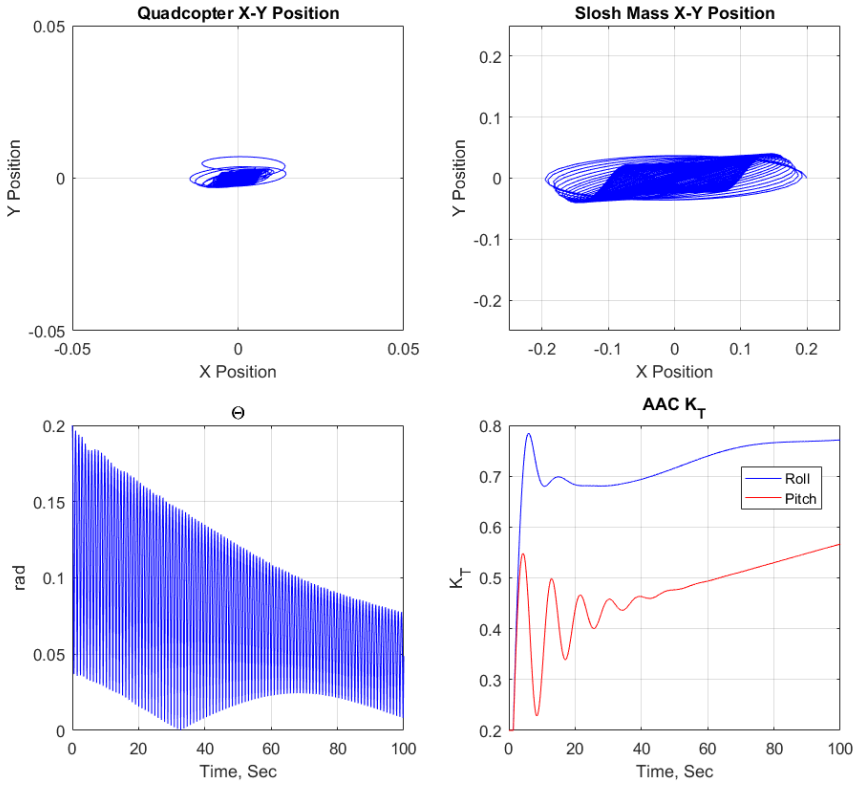

Figure 14. gain shift parameter = 2.3, AAC ON

B. Experimental Results

The ability of the AAC to suppress slosh instability on the quadcopter testbed in real-time was demonstrated at the indoor flight arena. The experiment was conducted as follows: 1) Takeoff, 2) Allow the quadcopter to maneuver its way to the center of the flight arena and the transients to settle, 3) Gradually bump up the "gain shift" parameter until instability (large amplitude oscillation in the hanging mass) was observed, 4) Flip the switch to allow the AAC to modulate the forward loop gain.

Figures 15 to 17 show results from a single experiment. The vertical dashed line at T = 100 seconds indicates the instance the AAC switch was flipped. Note: prior to T = 100 seconds, the AAC was still running but not fed into the control signal. The test officially started at T = 50 seconds after takeoff and the associated settling period. The outer loop "gain shift" parameter was gradually increased to 2 during the first 20 seconds. During this time frame, the slosh mass started to exhibit the rotary slosh behavior and the amplitude of oscillation grew to nearly 20 degrees. For the next 30 seconds, the "gain shift" parameter remained at 2 and oscillations hovered around 20 degrees. The baseline controller was having difficulties holding constant attitude and the system was clearly unstable. The AAC algorithm sensed this instability and dropped K_T way below 1 but was not fed into the control signal. At T = 100 seconds the AAC switch was activated and instability was suppressed within the first 10 seconds. The slosh mass amplitude dropped to an average of 5 degrees and the quadcopter attitude error stayed close to zero for the remainder of the experiment. The sudden spike in the AAC pitch channel at around T = 130 seconds appears to be the quadcopter responding to a dropout in the Vicon measurements and manifested itself in the attitude error and slosh mass angle histories.

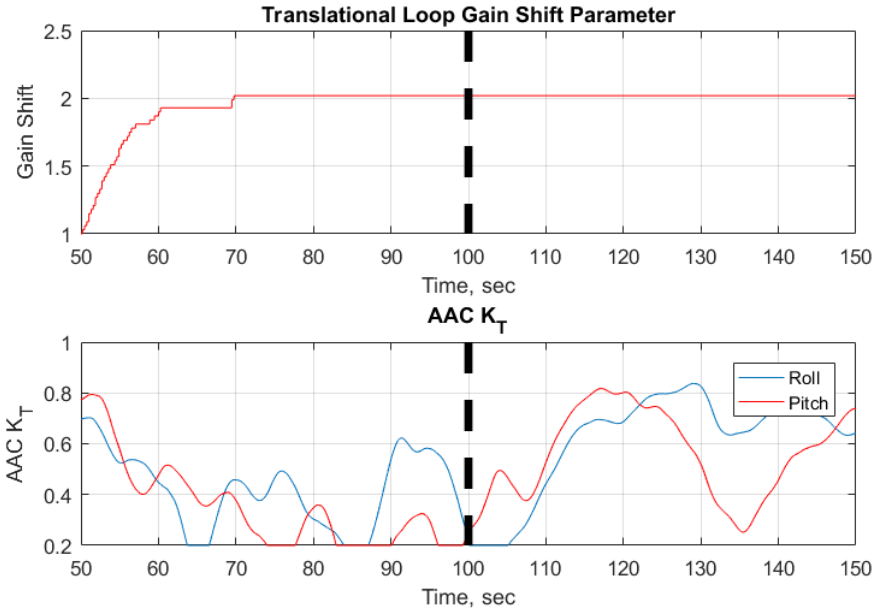

Figure 15. Flight Test Gains

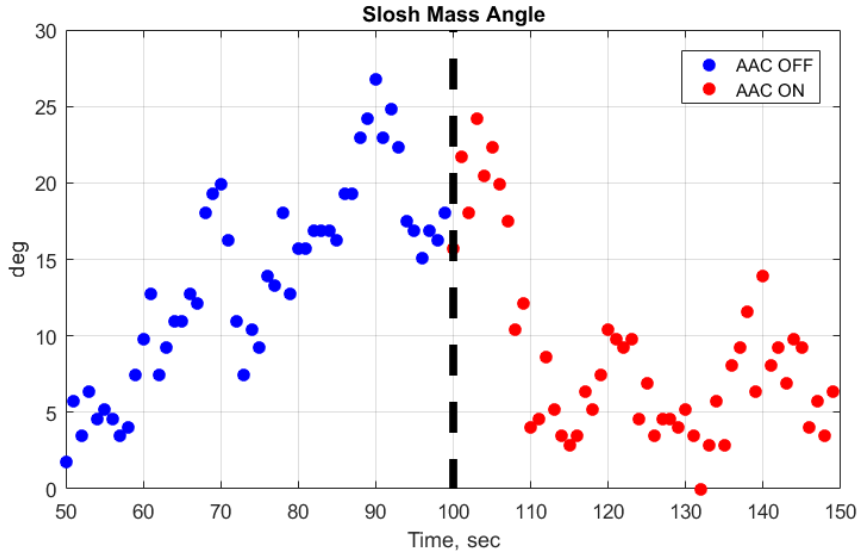

Figure 16. Flight Test Slosh Mass Amplitude

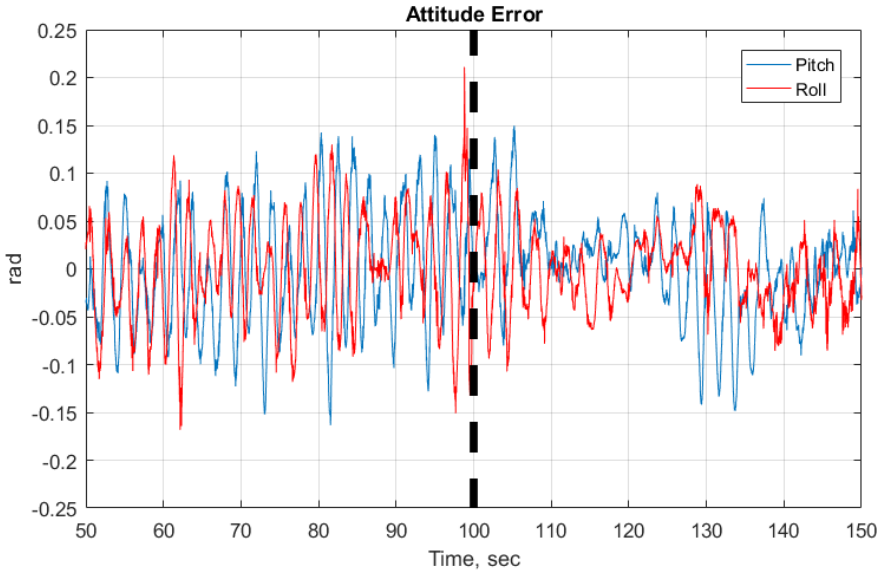

Figure 17. Flight Test Attitude Error

VI. Conclusion

In this study, a quadcopter plus hanging mass configuration was used to mimic the rotary slosh behaviors of liquid propellant inside a cylindrical tank onboard a launch vehicle. The two systems are dynamically similar in that the objective of the controller is to stabilize the vehicle and respond to guidance commands while suppressing the undesirable effects of slosh dynamics. The ability of the SLS Augmenting Adaptive Control (AAC) in response to slosh instability was demonstrated by intentionally driving the slosh mass onboard the quadcopter. The algorithm successfully suppressed the slosh instability in real time. Overall, this classroom type of exercise was successful in demonstrating the applicability of the AAC algorithm and provides further confidence in the design.

VII. Acknowledgments

The authors would like to thank Dr. Danette Allen for granting access to the Autonomy Incubator, the NASA Langley Aeronautics Academy Program and the NASA Engineering Safefy Center (NES&C) Flight Mechanics Technical Discipline Team for funding support. Helpful technical reviews were performed by John Wall, John Ottander, and Dr. Carlos Roithmayr.

References

[1]Bauer, H., "Stability Boundaries of Liquid-Propelled Space Vehicles with Sloshing," *AIAA Journal*, Vol. 1, No. 7, July. 1963.

[2]SpaceX, "Falcon Demo Flight 2. Flight Review Update," Tech. rep., SpaceX, July 2007.

[3]Greensite, A., "Analysis and Design of Space Vehicle Flight Control Systems. Volume VII. Attitude Control During Launch," Tech. Rep. CR-826, NASA Contractor Report, July 1967.

[4]Orr, J., "State Space Implementation of Linear Pertubation Dynamic Equations for Flexible Launch Vehicles," No. 2009-5962, AIAA, 2009.

[5]Gandhi, P., "Active Stabilization of Lateral and Rotary Slosh in Cylindrical Tanks," IEEE, 2010.

[6]Miles, W., "Stability of Forced Oscilllations of a Spherical Pendulum," Quart Applied Math, 1962.

[7]Dodge, F., "The New Dynamic Behavior of Liquids in Moving Containers," Tech. rep., Southwest Research Institute, 2000.

[8]Thomson, W. T., *Introduction to Space Dynamics*, Dover Publications, 2nd ed., 1986.

[9]Pei, J. and Rothhaar, P., "Demonstration of Launch Vehicle Slosh Instability on a Pole-Cart Platform," No. 2015-2712, AIAA, 2015.

[10]Orr, J. and VanZwieten, T., "Robust, Practical Adaptive Control for Launch Vehicles," No. 2012-4549, AIAA, 2012.

[11]VanZwieten, T., Gilligan, E., Wall, J., Orr, J., Miller, C., and Hanson, C., "Adaptive Augmenting Control Flight Characterization Experiment on an F/A-18," No. AAS 14-052, AAS, 2014.

[12]VanZwieten, T., Hannan, M., and Wall, J., "Evaluating the Stability of NASA's Space Launch System with Adaptive Augmenting Control," ESA GNC, 2017.

[13]Wall, J., Orr, J., and VanZwieten, T., "Space Launch System Implementation of Adaptive Augmenting Control," No. AAS 14-051, AAS, 2014.

[14]Wall, J., VanZwieten, T., Gilligan, E., Miller, C., Hanson, C., , and Orr, J., "In-Flight Suppression of a Destabilized F/A-18 Structural Mode Using the Space Launch System Adaptive Augmenting Control System," No. 2015-1775, AIAA, 2015.

[15]"Space Launch System Program Integrated Guidance, Navigation, and Control Performance Assessment Volume 4," Tech. rep., NASA, March 2015.

[16]Pei, J. and Rothhaar, P., "Demonstration of the Space Launch System Augmenting Adaptive Control Algorithm on Pole-Cart Platform," No. 2018-0608, AIAA, 2018.

[17]Miller, L., Pei, J., and Rothhaar, P., "Demonstration of the Space Launch System Augmenting Adaptive Control Algorithm on a Quad-rotor," No. 2018-0609, AIAA, 2018.

[18]Shaub and Junkins, *Analytical Mechanics of Space Systems*, AIAA, 2003.

[19]Kana, D., "A Model for Nonlinear Rotary Slosh in Propellant Tanks," *AIAA Journa of Spacecrafts*, Vol. 26, No. 2, May-June 1989, pp. 188–195.

[20]Hoffmann, G., Haomiao, H., Waslander, S., and Tomlin, C., "Quadrotor Helicopter Flight Dynamics and Control: Theorey and Experiment," No. 2007-6461, AIAA, 2007.

[21]Vicon Motion Systems Limited, *Vicon Tracker Guide*, March 2013.

[22]Jang, J., Hall, R., Bedrossian, N., and Hall, C., "Ares-I Bending Filter Design Using A Constrained Optimization Approach," No. 2008-6289, AIAA, 2008.

[23]Frosh, J. and Vallely, D., "Saturn AS-501/S-IC Flight Control System Design," *AIAA Journa of Spacecraft*, Vol. 4, No. 8, August 1967.

[24]Real-Time Innovations Inc., *RTI Connect DDS User Manual*, June 2015.

[25]Intel Developer Zone, *Intel Edison Board User Guide*, June 2017.